NDT&E International 52 (2012) 76–85

Contents lists available at SciVerse ScienceDirect

NDT&E International

journal homepage: www.elsevier.com/locate/ndteint

Monitoring the hydration of cement using highly nonlinear solitary waves

Xianglei Ni [a], Piervincenzo Rizzo [a,*], Jinkyu Yang [b,c], Devvrath Katri [b], Chiara Daraio [b]

[a] Laboratory for Nondestructive Evaluation and Structural Health Monitoring Studies, Department of Civil and Environmental Engineering, University of Pittsburgh, Pittsburgh, PA 15261, USA

[b] Engineering and Applied Science, California Institute of Technology, 1200 E California Boulevard, MC 105-50, Pasadena, CA 91125, USA

[c] Department of Mechanical Engineering, University of South Carolina, 300 Main Street, Room A220, Columbia, SC 29208, USA

ARTICLE INFO

Article history:
Received 8 June 2011
Received in revised form
1 May 2012
Accepted 9 May 2012
Available online 22 May 2012

Keywords:
Highly nonlinear solitary waves
Cement
Hydration
Nondestructive evaluation

ABSTRACT

In this paper we present a nondestructive evaluation technique based on the propagation of highly nonlinear solitary waves (HNSWs) to monitor the hydration of cement. HNSWs are mechanical waves that can form and travel in highly nonlinear systems, such as one-dimensional chains of contacting spherical particles (i.e., granular crystals). In the present study, we use a granular crystal-based actuator/sensor to observe the solitary waves propagating to and from the mechanical interface between the transducer and a fresh gypsum cement sample. We hypothesize that the reflected HNSWs traveling along the crystal-based transducer are affected by the hydration process of the cement, and we assess the elastic modulus of the specimen in the localized region of the granular crystal contact. To verify the experimental results, we perform numerical simulations based on a simplified finite element model. The elastic properties of the cement specimen measured by the granular crystal transducer are compared with the compressive strength and the elastic modulus measurements obtained from destructive tests, conducted according to the ASTM C109. We observe good agreement between experiments and numerical simulations.

1. Introduction

The quality and the durability of cement-based products are influenced by early stages of hydration [1,2]. The observation of the hydration process permits to predict the long-term behavior of cement-based materials, and to accurately estimate their setting time [3,4]. In the past 20 years, several nondestructive evaluation (NDE) techniques have been proposed to monitor the hydration of cement. These methods correlate certain mechanical, electrical, or acoustical parameters with the cement or concrete properties by using empirical relationships [5]. The most widely-used NDE technique is based on the propagation of ultrasounds [3,4,6–19]. Other methodologies make use of electromagnetic waves [20,21], electrical resistivity [18], and X-ray diffraction [14].

The schematic of ultrasonic-based methods is presented in Fig. 1. In these methods, cement samples are typically inspected by commercial transducers that generate longitudinal [4,7,8–10,14–16,18,19] or longitudinal and shear [3,11,12] bulk waves. Parameters such as wave speed and attenuation are then measured and empirically correlated to the cement material properties. This approach is usually referred to as the ultrasonic pulse velocity (UPV) method [22] (Fig. 1a). To obtain good signal-to-noise ratio, longitudinal wave transducers cannot be used to generate transverse waves and vice versa. Thus, to use both shear and longitudinal waves, at least four transducers are necessary. The approach is feasible if the access to the back-wall is possible and the exact distance between the transducers is known and kept constant during the measurement. Furthermore, the contact conditions between the transducers and the cement surface must be kept constant. If the access to the back wall of the sample is not practical, the wave reflection method can be adopted (Fig. 1b). In this approach, the reflection loss of ultrasonic shear [6,13] or longitudinal [4,16,21] waves at an interface between a buffer material, typically a steel plate, and the cementitious material is monitored over time. The amount of wave attenuation depends on the reflection coefficient, which in turn is a function of the acoustical properties of the materials that form the interface [5].

In this paper, we propose a NDE approach to monitor cement hydration at early age based on the use of highly nonlinear solitary waves (HNSWs). HNSWs are mechanical waves that can form and travel in highly nonlinear systems, such as a closely packed chain of elastically interacting particles (also called a granular crystal) [23–35]. The most common way to induce the formation of solitary waves is by impacting the first particle of the granular chain with a striker. The impact velocity and the mass of the striker determine the characteristics of the traveling HNSWs in terms of number of pulses forming, speed, amplitude, and

* Corresponding author. Tel.: +1 412 624 9575.
E-mail address: pir3@pitt.edu (P. Rizzo).

0963-8695/$ - see front matter © 2012 Elsevier Ltd. All rights reserved.
http://dx.doi.org/10.1016/j.ndteint.2012.05.003

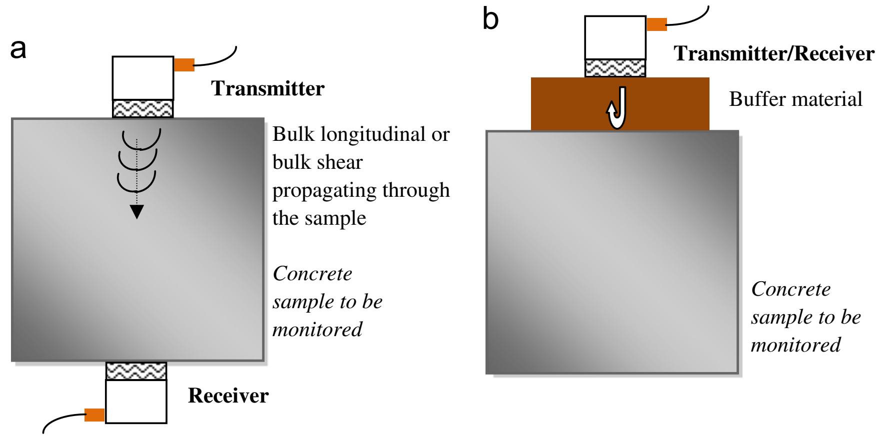

Fig. 1. (a) UPV approach. Two L transducers or S transducers are used to transmit and receive bulk waves. Wave speed and amplitude are measured. (b) Wave reflection method. One L- or S-transducer is used in the dual-mode, i.e., as both transmitter and receiver. A buffer material is interposed between the transducer and the concrete.

duration. In this study, we transmit a single HNSW to the interface between the granular chain and a cement sample. We propose to monitor the hydration process of the cement sample by measuring the reflected waves formed at the actuator/cement interface.

The interaction of HNSWs with linear systems was studied earlier [32–35]. Manciu and Sen [32] investigated the wave reflections from rigid wall boundaries. Falcon et al. [33] studied the fragmentation of a chain of particles (beads) when impacting a fixed wall. Job et al. [34] evaluated the collision of a single solitary wave with elastic walls of various hardness. Yang et al. [35] studied the interaction of HNSWs with uniform and composite elastic media. It was shown that the formation and propagation of reflected HNSWs are highly dependent on the elastic modulus and geometry of the adjacent medium. These studies suggest that HNSWs are excellent information carriers for the nondestructive assessment of materials and structures.

Recently, we have designed, built, and tested an actuator/sensing system, hereafter indicated as HNSW transducer, to generate and detect solitary waves in an efficient and controllable manner [31]. In the present study, we use this transducer to generate HNSWs and to measure the amplitude and travel time of the waves reflected from the cement surface. The experimental results are compared to a simplified finite element (FE) model using Abaqus. We validate the proposed HNSW-based diagnostic scheme by matching the predicted elastic properties of the cement sample with the results of the ultimate compressive strength and Young's modulus values obtained by destructive testing conducted in accordance to the ASTM C109 [36]. The experimental results from the proposed NDE method are in good agreement with numerical data, and they also show strong correlation with the measured mechanical properties obtained from the ASTM C109.

With respect to the use of ultrasounds, the novelty and the advantage of this HNSW-based NDE technique is multifold: (1) it exploits the propagation of HNSWs in granular systems ignoring the stress wave propagation across the cement; (2) it employs a cost-effective actuator/sensor that does not require the use of arbitrary function generators; (3) it measures several waves' parameters that can be used to correlate multiple cement variables; (4) it does not require, unlike UPV method, the knowledge of the distance between a transmitter and a receiver and does not require the access to the sample's back-wall.

The paper is organized as follows. The general principles of the proposed methodology are presented in Section 2. This includes short formulation of the equations governing the propagation of HNSWs in granular materials and the description of the transducer used in the experiments. Section 3 describes the experimental setup. The setup and the results of the numerical model are presented in Section 4. As the numerical model was designed to simulate the experiment, we discuss the FE analysis after the description of the experimental setup. Section 5 describes the results of the experiments performed in this study. The results are summarized in the conclusions.

2. Background

2.1. Highly nonlinear solitary waves

A brief introduction to the equations governing the propagation of HNSWs in a one-dimensional chain of spherical particles is given here. The formulation follows the notation adopted by the authors in [37]. The interaction between two adjacent identical beads is governed by Hertz's law [24,25]:

$$F = A\delta^{3/2}, \tag{1}$$

where F is the compression force between granules, δ is the closest approach of particle centers and A is coefficient given by:

$$A = \frac{E\sqrt{a}}{3(1-\nu^2)}. \tag{2}$$

In Eq. (2) a is the diameter of the beads, and ν and E are the Poisson's ratio and Young's modulus of the material constituting the particles, respectively.

The combination of this nonlinear contact interaction and a zero tensile strength in the chain of spheres leads to the formation and propagation of compact solitary waves [24]. In the long wavelength limit, when the wavelength is much larger than the particles' diameter, the speed of the solitary waves V_S depends on the maximum dynamic strain ξ_m [24] which, in turn, is related to the maximum dynamic force F_m between the particles in the discrete chain [28]. When the chain of beads is under a static pre-compression force F_0, the initial strain of the system is referred to as ξ_0. The speed of the solitary wave V_s has a nonlinear dependence on the normalized maximum strain $\xi_r = \xi_m/\xi_0$, or on the normalized force $f_r = F_m/F_0$ in the discrete case. Such a relationship is expressed by the following equation [28]:

$$V_S = c_0 \frac{1}{(\xi_r - 1)} \times \left\{ \frac{4}{15} \left[3 + 2\xi_r^{5/2} - 5\xi_r \right] \right\}^{1/2}$$
$$= 0.9314 \left(\frac{4E^2 F_0}{a^2 \rho^3 (1-\nu^2)^2} \right)^{1/6} \frac{1}{(f_r^{2/3} - 1)} \left\{ \frac{4}{15} \left[3 + 2f_r^{5/3} - 5f_r^{2/3} \right] \right\}^{1/2} \tag{3}$$

where c_0 is the wave speed in the chain initially compressed with a force F_0 in the limit $f_r=1$, and ρ is the density of the material. When f_r (or ξ_r) is very large, Eq. (3) becomes:

$$V_S = 0.6802\left(\frac{2E}{a\rho^{3/2}(1-\nu^2)}\right)^{1/3} F_m^{1/6} \tag{4}$$

which represents the speed of a solitary wave in a "sonic vacuum" [24,28].

The shape of a solitary wave with a speed V_s in a "sonic vacuum" can be closely approximated by [24]:

$$\xi = \left(\frac{5V_s^2}{4c^2}\right)\cos^4\left(\frac{\sqrt{10}}{5a}x\right), \left|\frac{\sqrt{10}}{5a}x\right| \le \frac{\pi}{2} \tag{5}$$

where

$$c = \sqrt{\frac{2E}{\pi\rho(1-\nu^2)}} \tag{6}$$

and x is the coordinate along the wave propagation direction. This mathematical expression represents a single pulse of highly nonlinear solitary waves confined within the width of approximately five particle diameters ($5\pi a/\sqrt{(10)} \sim = 5a$).

2.2. HNSW-based diagnostic principle

The general concept of the proposed technique is summarized in Fig. 2. A HNSW-based transducer, here schematized with a chain of identical beads, is in contact with the cement paste to be monitored. A thin aluminum sheet is placed in between the transducer and the cement to prevent the penetration of the bottom sphere inside the paste when fresh. The impact of a striker, having mass equal to that of the other particles composing the chain, generates a single HNSW that propagates through the chain and is partially reflected at the interface [23–28]. When the material adjacent to the granular chain is "hard" (e.g., has high values of Young's modulus) a single, strong HNSW is reflected from the interface. However, when the material adjacent to the granular chain is "soft" multiple HNSW can be generated at the interface [33–35]. We monitor the waves reflected from the transducer/cement interface using instrumented particles, hereafter indicated as sensor beads, inserted in the chain. The characteristics of the reflected pulses in terms of their amplitude, time-of-flight, and speed are correlated to the mechanical properties of the underlying cement paste. Besides the change of HNSWs caused by the mechanical conditions of the underlying layers, the waves can be tuned by changing the geometry or mechanical properties of the particles. For instance, by enlarging the particles size the spatial wavelength increases, and the wave speed and amplitude decrease. By augmenting either the mass of the striker or the precompression force, both the amplitude and the wave speed increase. This tunability can be exploited to replace some of the electronic equipment, such as function generators, conventionally utilized to excite stress waves of specific shape and wavelength. This represents another advantage of the present technology with respect to the ultrasonic-based NDE methods.

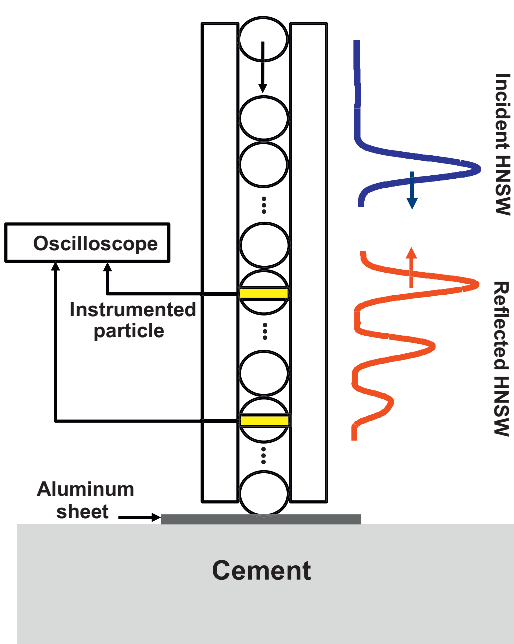

Fig. 2. Schematic of the proposed HNSW-based NDE approach. A chain of spherical particles is placed on the surface of the cementitious material to be monitored. The chain acts as an actuator for the generation of HNSWs and as a sensor to detect the solitary waves reflected from the interface between the chain and the material. A thin aluminum plate is interposed between the chain and the object to prevent the collapse of the bottom particles inside the fresh cement.

When a single HNSW interacts with a "soft" neighboring medium, secondary reflected solitary waves (SSW) form in the granular crystal, in addition to the primary reflected solitary waves (PSW) [33–35]. In this paper, we hypothesize that these reflected waves are strongly influenced by the mechanical properties of the cement specimens under inspection. The stiffness of the linear medium indirectly affects the dynamic contact force F_m of the reflected waves that, in turn, influences the speed of the reflected solitary wave as described in Eq. (3).

We characterize the wave reflection properties measuring the time-of-flight (TOF), the amplitude ratio of the primary reflected solitary wave (ARP), and the amplitude ratio of the secondary reflected solitary wave (ARS). Here, the TOF denotes the transit time at a given sensor bead in the granular crystal between the incident and the reflected waves. We define the ARP as the ratios of the PSW amplitude divided by the incident solitary wave amplitude and the ARS as the ratio between the SSW amplitude and the incident wave amplitude.

2.3. HNSW transducer

For the generation and detection of HNSWs, a simple cost-effective transducer (Fig. 3a and Fig. 3b) was designed and built [31]. It consisted of a polytetrafluoroethylene tube having inner diameter equal to 4.8 mm, filled with 20 type-302 stainless steel beads. The diameter of each sphere was 4.76 mm and the mass was 0.45 g. Two sensor beads were assembled to detect the propagating solitary waves (the sensors are similar to the one used in [26–28]). Fig. 3c shows a photo of a sensor bead. The instrumented particle consisted of a piezo-gauge made from lead zirconate titanate (square plates with 0.27 mm thickness and 2 mm width) embedded inside two steel half particles. The piezo-gauge was equipped with nickel-plated electrodes and custom micro-miniature wiring. The procedure used to assemble and calibrate the instrumented particles was similar to that described in [24,26,34,37,38]. The sensor beads were positioned along the chain at the 11th and 16th position from the top. The location of the instrumented particles is determined by the following considerations. First, the consolidation of the HNSWs is complete approximately 5 beads away from the impact. Second, the sensor cannot be located too close at the interface with the linear medium because the force profile would be affected by the interference of the incident and reflected waves.

The striker consisted of a low-carbon steel bead having a diameter of 4.76 mm and a mass of 0.45 g. We employed the low-carbon steel material to control the motion of the striker using an electromagnet connected to a DC power supply. The electromagnet

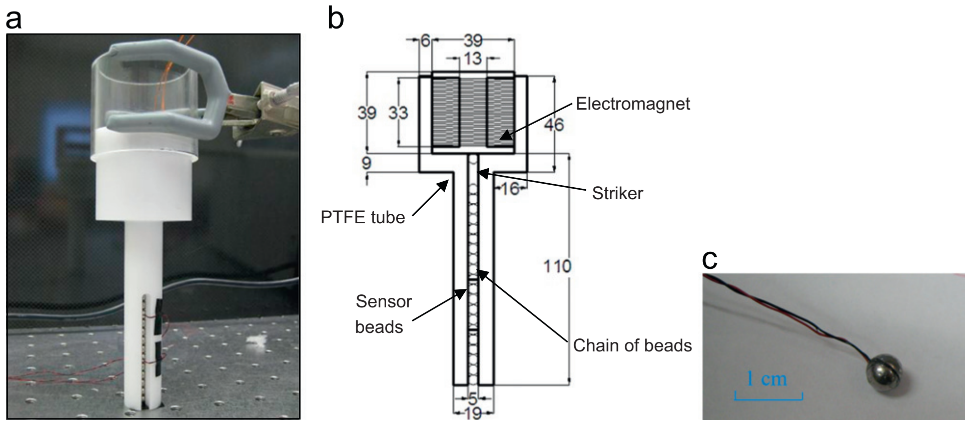

Fig. 3. (a) Photo of the HNSW transducer for the remote non-contact generation of HNSWs. A mechanical grip is used to hold the transducer during the experiments presented here. (b) Schematic diagram of the HNSW transducer. Dimensions are in mm. Figures reprinted with permission from [31]. (c) Photo of a typical instrumented particle devised for the detection of the propagating solitary waves.

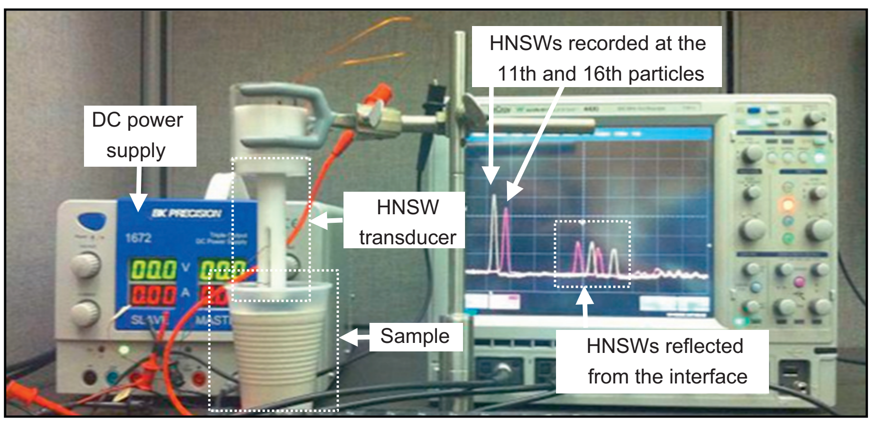

Fig. 4. Photo of the experimental setup. The HNSW transducer is positioned on the gypsum cement sample, and a DC power supply is connected to the electromagnet inside the HNSW transducer. Two instrumented sensors at the 11th and 16th particle positions in the HNSW transducer measure force profiles of reflected waves, which are digitized and stored by a connected oscilloscope.

was placed on the top of the tube to lift the striker to 5.5 mm above the chain. A detailed description of the transducer and its ability to generate repeatable HNSWs is reported in [31].

3. Experimental setup

To evaluate the proposed NDE methodology, we prepared one conical frustum sample of fast setting USG® Ultracal 30 gypsum cement. This material is a low expansion rapid-setting gypsum cement used in the building industry as a surface finish of interior walls and in the production of drywall products for interior lining and partitioning. In our experiment we prepared a paste with water and cement in a ratio of 0.38, as recommended by the manufacturer. The paste was poured into a plastic mold after 5 min of mixing. The conical frustum sample obtained from the mold was 77 mm high, with top and bottom diameters equal to 62 mm and 42 mm, respectively (Fig. 4). A $40 \times 40 \times 0.254$ mm aluminum sheet was placed on top of the specimen 30 min after pouring the paste in the mold, and the granular chain actuator was placed on top of the sheet 7 min later. A DC power supply provided current to activate the electromagnet located on the top of the granular chain. Instrumented sensor particles inserted in the chain measured the incident and reflected HNSWs, which were recorded by an oscilloscope. The signals were digitized at 5 MHz sampling rate. Five measurements were taken every three minutes during the first 90 min of the cement age. Then, five measurements were recorded every 6 min until cement age was 180 min. Monitoring was stopped 3 h after mixing, in accordance to the manufacturer's nominal setting time.

4. Numerical setup and results

The experimental setup was simulated using an axisymmetric FE model in Abaqus [30,39–40]. The model studied the coupling behavior between a granular crystal and cement, focusing on the contact interface. We assumed that the cementitious material properties in the localized region of inspection are approximately uniform. As such, we used a simplified approach that considers the cement paste as an elastic, isotropic, and homogeneous medium. We did not include dissipation in this FE model, although its presence in granular crystals has been demonstrated in the past [41]. The model included the granular chain, the aluminum layer, and the cement paste (Fig. 5). Under the assumption of small deformations, the spherical particles in the chain were modeled as axisymmetric elastic bodies. The dimensions of the spherical particles and the conical cement sample used in the model were identical to those of the experiment. To preserve axisymmetric assumptions, we modeled the aluminum sheet as a 40 mm-diameter disk instead of the square sheet used in the experiment. All the components were discretized using

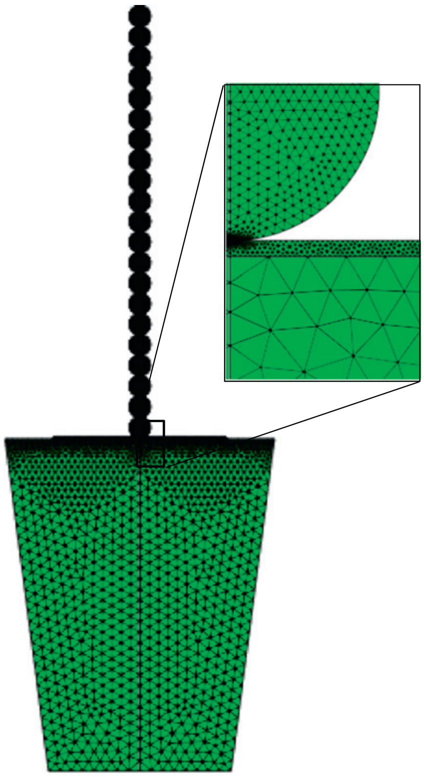

Fig. 5. Axisymmetric finite element model of the experimental setup, including the granular chain, the aluminum sheet and the conical frustum gypsum sample. The inset shows the magnified view of the sphere contact with the aluminum plate and the gypsum cement using 6-noded triangular meshes. A fixed boundary condition is applied to the bottom of the cement paste.

Table 1
Mechanical properties of materials used in the experiments.

Material	Density [kg/m^3]	Young's modulus [GPa]	Poisson's ratio
Stainless steel AISI type 302	7800	200	0.28
Aluminum alloy 1100	2700	70	0.33
Gypsum cement	2250	0.002–20	0.30

axisymmetric 6-node second-order triangular elements, and we used the material properties listed in Table 1. To get a better representation of the contact interaction, a denser mesh was employed in the vicinity of the contact point (inset of Fig. 5).

The impact of the striker was simulated by considering the striker in contact with the top particle and setting its initial velocity v_0 equal to $v_0 = \sqrt{2gh}$, where g is the gravitational constant and h is the height of the falling bead (h=5.5 mm).

To simulate cement hardening from fresh to completely cured status, we varied the Young's modulus of the sample over a wide range of values (from 0.002–20 GPa). Fig. 6 shows the temporal force profiles computed at the 11th particle, when an incident solitary wave interacted with samples of different elastic moduli. The signals obtained for each run are shifted vertically to ease visual comparison. The first pulses in the force profiles represent the incoming solitary waves arriving at the sensor bead, while the rest of the pulses are the PSW and SSW reflected from the interface. Clearly, the TOF of both reflected waves is strongly dependent on the sample's modulus of elasticity. As the stiffness of the sample increases, the amplitude of the PSW increases, while the TOF of the PSW decreases.

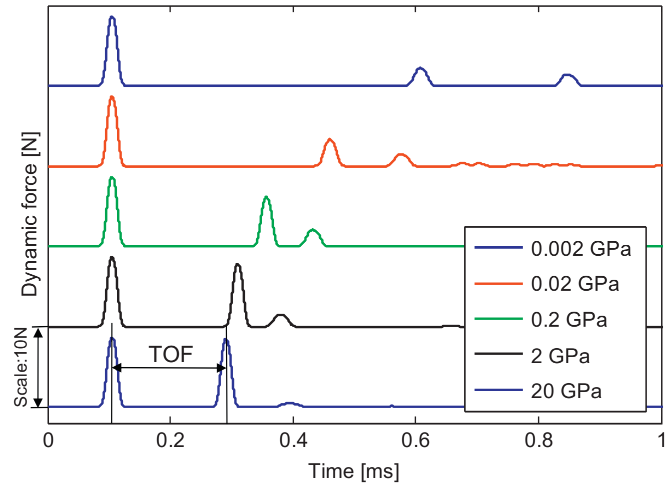

Fig. 6. FEM simulation of HNSW interaction with gypsum cement samples in various elastic condition. All signals represent propagating waves through the 11th bead in the chain. To ease visualization, the signals are shifted by 10 N in the vertical axis. The time of flight (TOF) values of HNSWs are extracted by measuring the time elapsed between the incident (the leftmost impulses) and the first reflected wave (subsequent impulses).

Fig. 7 shows the TOF as a function of the sample's elastic modulus for the primary (circular blue line) and secondary (square red line) reflected solitary waves. For both waves, the TOF decreases as the elastic modulus of the gypsum increases (by almost 68% for PSW and 58% for SSW). This means that more rehydrated gypsum cements (i.e., harder samples) generate faster reflection of solitary waves from the interface between the actuator and the cement. The TOF trend of the secondary solitary waves follows closely to that of the PSW with approximately 0.1 to 0.2 ms offset. The variation of the TOF becomes less sensitive to the mechanical properties of the adjacent medium once the Young's modulus of the material reaches the value of 1 GPa. We observe a slight increase of the TOF values for the SSWs, given the cement's elastic modulus higher than 1 GPa. This can be explained by the amplitude-dependent nature of solitary waves' speed [Eq. (4)]. We will discuss this trend in the later part of this section.

The velocities of incident and primary and secondary reflected solitary waves are shown in Fig. 7(b) as a function of the cement's elastic modulus. This speed is calculated by measuring the transit time of the propagating waves between the 11th and 16th particles of the chain. The green line with crosses in Fig. 7(b) refers to the incoming signals that exhibit identical pulses with constant velocity. The blue line with circles represents the propagation speed of PSW. We find that the PSW speed is increased by 26%, from 413 m/s to 522 m/s (circular blue line), as the cement's elastic modulus changes from 2 MPa to 20 GPa. This implies that the "hard" cementitious interface results in larger reflection speed of PSWs, compared to those against "soft" cementitious media. The velocity profile of SSWs shows an approximately parabolic trend. This is qualitatively consistent with the TOF trend in Fig. 7(a), showing a critical point in the curve.

It is notable that the propagation speed of reflected HNSWs varies in response to the cement's material properties. This is in sharp contrast to conventional NDE approaches based on linear elastic waves, where the velocity of the reflected waves is generally independent of the underlying material properties, and materials information can only be extracted from variation of amplitude of the reflected waves. The HNSW-based evaluation method can use both amplitude-related and velocity-related

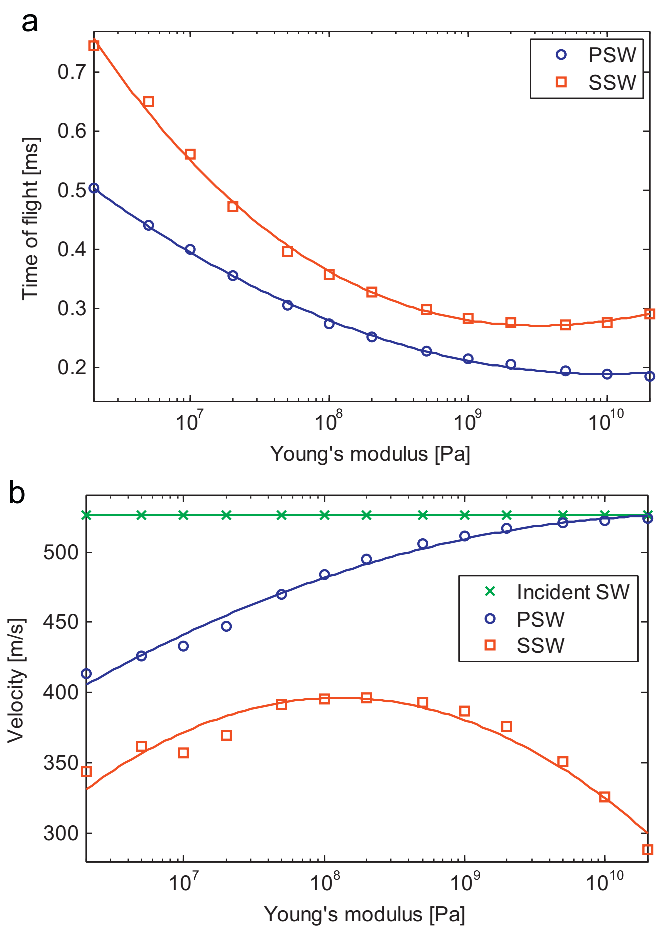

Fig. 7. Numerical results showing time of flight and propagating speed of HNSWs. Solid lines represent fitted curves based on polynomial least square method. (a) Time of flight of the primary (circular blue dots) and secondary (square red dots) reflected solitary waves as a function of the cement's elastic modulus. (b) Velocity of incident (crossed green dots) and primary reflected (circular blue dots) solitary waves. (For interpretation of the references to color in this figure legend, the reader is referred to the web version of this article.)

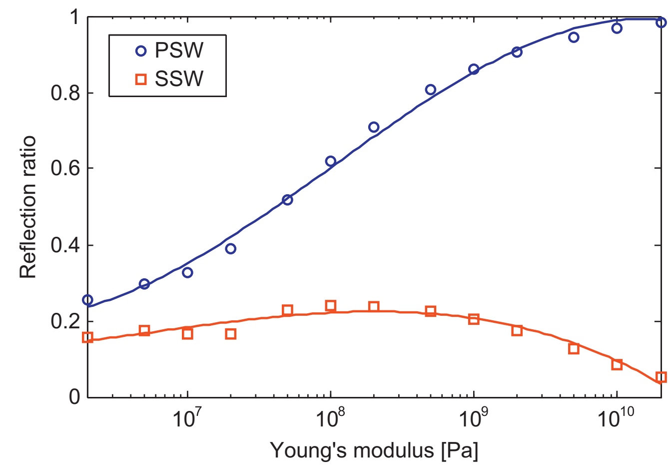

Fig. 8. Numerical results showing amplitude ratios of the primary (circular blue dots) and secondary (square red dots) reflected solitary waves as a function of the cement's elastic modulus. Solid lines are based on polynomial curve-fitting using least square method. (For interpretation of the references to color in this figure legend, the reader is referred to the web version of this article.)

features of the reflected pulses, and can therefore be more sensitive than conventional wave reflection methods.

Fig. 8 illustrates the ARP and ARS as a function of the sample's elastic modulus. When the effective stiffness of the cement paste increases, the amplitude ratio of the PSW increases from 0.25 to approximately 1 (blue line with circles). This translates into stronger repulsion of the HNSW at the interface, when the HNSW transducer interacts with stiffer cement samples. The ARS does not exhibit a monotonous behavior (see the red line with squares in Fig. 8). This is due to the complex particles dynamic occurring at the interface during the formation of the secondary solitary waves. When the stiffness of the cementitious interface is low, the amplitude of SSW is small due to the soft restitution of incident solitary waves. On the other hand, if the elastic modulus of the bounding medium is very high, the energy caused by the strong repulsion of incident waves is carried mostly by the PSWs, leaving a small portion of energy to the SSWs. This leads to negligible amplitude of SSWs against a stiff cementitious wall. We obtain a parabolic shape of the SSW velocity profile. This also explains the variation of SSW's TOFs in the high elastic moduli as shown in Fig. 7a. In summary, from these numerical results, it is evident that the proposed HNSW-based diagnostic scheme shows sensitivity to the hardened status of the cement, herein represented by its effective elastic modulus.

5. Experimental results

5.1. HNSW measurements

Fig. 9 shows the time history of the force measured by the 11th particle in the chain, at five different times of the hydration process. The top plot represents the HNSW profile after 45 min of curing process, while the bottom plot shows the force signal measured after 120 min of cement age. In this figure, the incident pulse and the primary and secondary reflected waves are clearly visible. We also observe that the shape, amplitude, and travel time of the reflected waves changed with cement age. It is notable that Fig. 9 is very similar to Fig. 6, implying a close relationship between cement's curing time and its elastic modulus. The variation of elastic modulus as a function of the curing time will be addressed in Section 5.3.

Fig. 10(a) shows the measured TOFs of both primary (blue line with circles) and secondary (red line with squares) reflected waves as a function of the hydration time. Each dot indicates the mean value of the five experimental measurements, and the vertical error bars represent the 95.5% (2σ) confidence interval. The barely visible error bars demonstrate the repeatability of the proposed methodology. The trend evident in Fig. 10(a) clearly denotes the presence of a two-stage evolution. In the first stage, lasting between 45 and 90 min, the TOF values of PSW and SSW decrease approximately exponentially. After 90 min the variation of the TOF plateaus, changing only slightly with increasing cement age. The trends observed in these results are well captured by the numerical data (see Fig. 7). Discrepancies between Figs. 7 and 10 (a) stem from the different physical parameters used in the horizontal axis and from the approximations used in the numerical model. Fig. 10(b) shows the wave speed of the incident solitary wave (green line with crosses) and the speed of both reflected waves as a function of curing time. Similarly to the analysis of the TOF, we find that the speed of the primary reflected wave becomes less sensitive to the materials properties of the cement, as the curing time progresses. We also observe that the incident wave velocity remains almost constant in all tests performed. The speed of the secondary reflected waves (SSW) measured experimentally appears to qualitatively disagree with what observed in numerical simulations. After ~120 min of curing time, the SSW speed measured experimentally remains constant, while in numerical simulations it decreases with

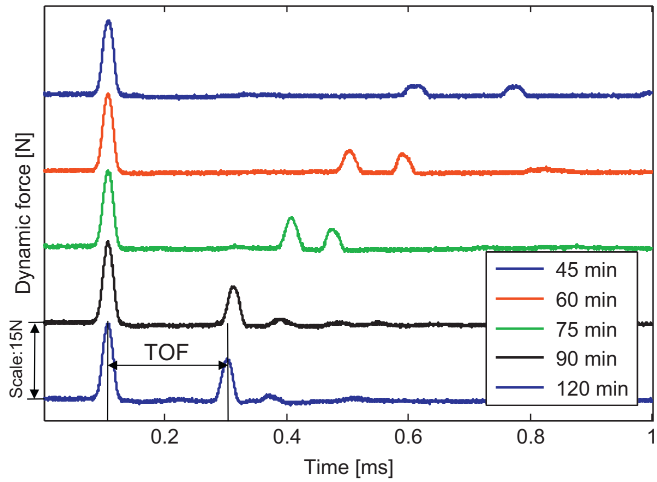

Fig. 9. Experimental results of HNSW interaction with gypsum cement samples in various cement age. The force profiles are measured from the 11th bead in the HNSW transducer.

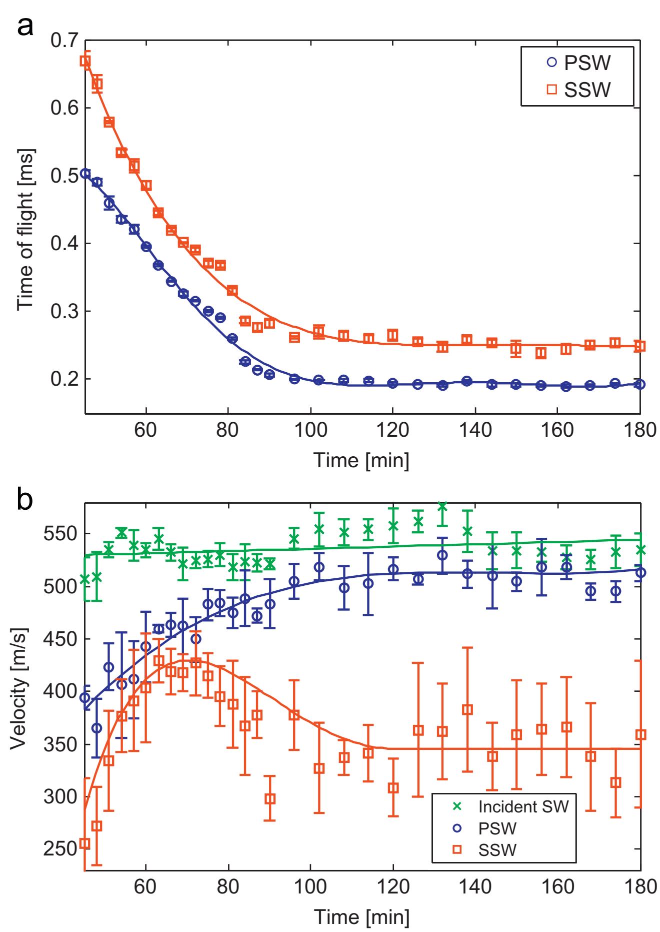

Fig. 10. Experimental results showing time of flight and propagating speed of HNSWs. The vertical error bars represent standard deviations obtained from five signal measurements, and the solid lines denote the fitted curves based on discrete measurement data. (a) TOF of the primary (circular blue dots) and secondary (square red dots) waves as a function of cement age. (b) Velocity of the incident (crossed green dots), primary reflected (circular blue dots), and secondary reflected (square red dots) HNSWs as a function of cement age. (For interpretation of the references to color in this figure legend, the reader is referred to the web version of this article.)

increasing Young's modulus of the cement. The explanation is multi-fold. First, the low signal-to-noise ratio associated with the SSW' force profile measured by both transducers makes it difficult to accurately estimate the arrival time. This is evident when the standard deviation is compared to the plot relative to the incident and the primary waves. Second, the time-of-flight includes the contact time of the bottom bead inside the cement. Finally, the numerical model over-predicts the speed of the secondary wave for the very fresh cement. This is probably due to the approximation of the finite element approach that considered the plaster linear and isotropic even at early stage.

The variations of the ARP and the ARS as a function of the cement age are shown in Fig. 11. While the amplitude ratio of the primary wave increases with cement age (blue line with circles), the ARS exhibits a relatively complex behavior during the curing process (square red line). The non-monotonic response of the SSW, predicted by the numerical results (Fig. 8) is evident. We speculate that during the first hour water bleeding might have increased the "flexibility" of the surface, enhancing the formation of the secondary waves. It is worth noting that the amplitude of the primary reflected wave has a four-fold increase with respect to the fresh cement.

5.2. Compressive strength test

Uniaxial compression tests were performed according to ASTM C109 using a Test Mark machine operated in displacement control. Eighteen 50-mm cubes were prepared using the water-to-cement ratio (0.38) suggested by the manufacturer. The paste mixture was blended 3 min prior to pouring into the molds. Each sample was removed from the mold before testing. Fig. 12 shows the measured compressive strength as a function of the hydration time. We observe that the cement strength increases drastically up to the cement age of 90 min and becomes approximately identical afterwards. This is in agreement with the behavior of extracted features from HNSWs, as observed in Fig. 10(a).

To compare the measured strength with the HNSW responses, we superimpose the plots of TOF and ARP on the top of the strength curve, as shown in Fig. 12(a) and (b), respectively. For the sake of comparison, we used "TOF variation" in Fig. 12(a), which represent the deviation of the measured TOF values from the TOF recorded at 65 min. As demonstrated in both Fig. 12(a) and (b), the overall trend of the reflected HNSWs matches well with the measured strength of cement specimens. This implies the ability of the HNSW-based NDE approach to capture the variation of the cement's compressive strength.

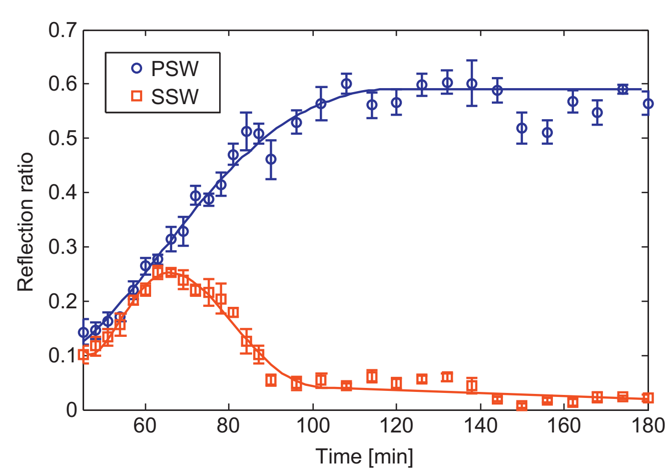

Fig. 11. Experimental measurements of amplitude ratios of the primary (circular blue dots) and secondary (square red dots) reflected solitary waves as a function of cement age. (For interpretation of the references to color in this figure legend, the reader is referred to the web version of this article.)

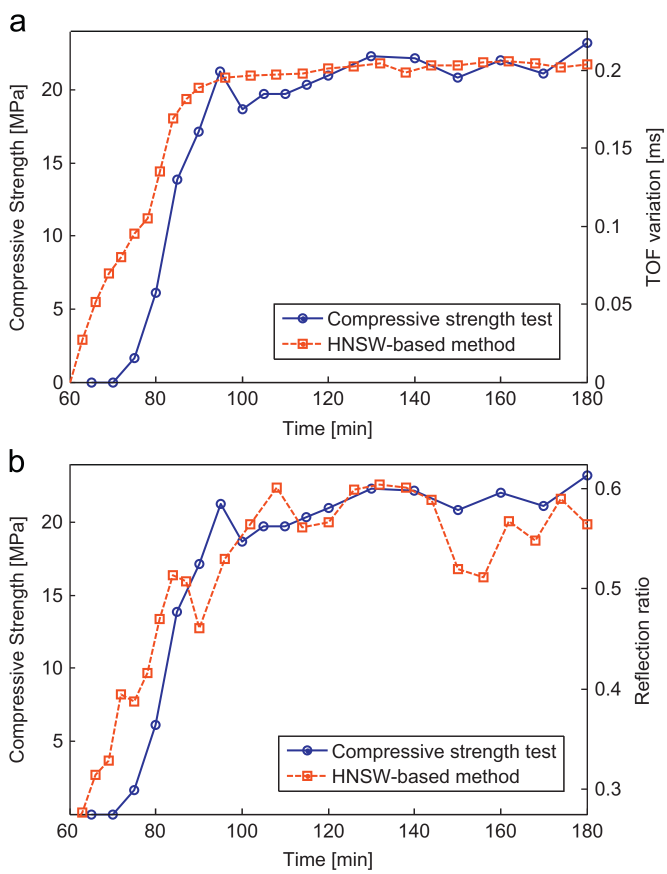

Fig. 12. Measurements of cement compressive strength as a function of the cement age. (a) Compressive strength superimposed to the TOF variation of the PSWs as recorded by the 11th bead. (b) Compressive strength superimposed to the amplitude ratio of the PSWs as measured by 11th bead. For the sake of clarity the error bars are removed from the plots of the HNSW-based features.

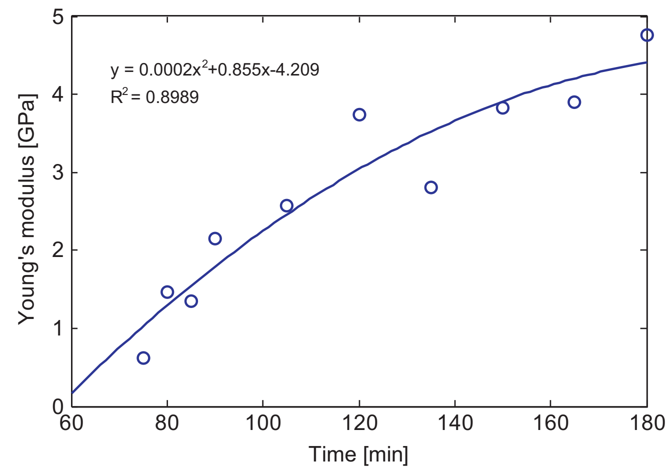

Fig. 13. Young's modulus of 50-mm cubic cement samples as a function of cement age. The circular blue dots represent measurement results based on a series of compression tests, while the solid blue line represents a fitted curve.

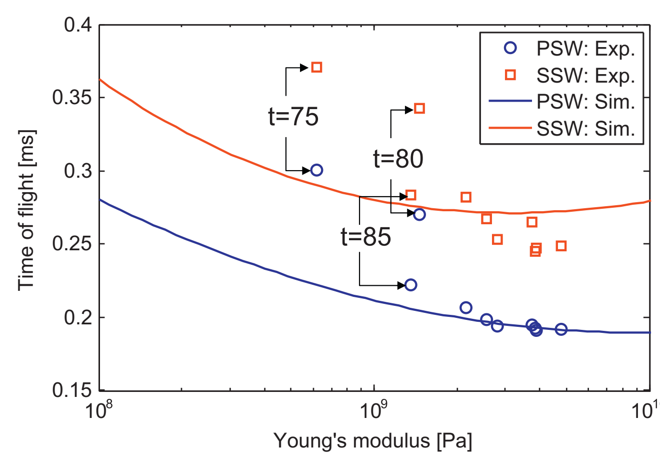

Fig. 14. Comparison of experimental and numerical data for the time of flight (TOF) as a function of the cement's elastic modulus. Numerical results of TOFs for the primary and secondary reflected waves are denoted by solid blue and red curves, while experimental measurements of PSW's and SSW's TOF values are represented by circular blue and square red dots, respectively.

5.3. *Young's modulus test*

To measure the elastic modulus of the cement paste, ten 50-mm cubes were tested with a Test Mark machine operated in displacement control. Both compressive force and displacement were recorded. The Young's moduli were extracted from the stress–strain curves and are shown in Fig. 13 as a function of the paste's age. We observe an increase of the measured Young's moduli for samples with higher cement age.

Based on the experimental relationship between the cement ages and their corresponding elastic moduli presented in Fig. 13, we can now describe the responses of HNSWs as a function of cement's elastic modulus. We first obtained the relation between the measured TOF and the Young's modulus as shown in Fig. 14. The numerical predictions in Fig. 7(a) are superimposed to the experimental values (blue curve for PSWs and red curve for SSWs). For the sake of clarity the results of the first three stiffness measurements (at 75, 80, and 85 min) are highlighted. It can be seen that the first two measurements show significant deviations from the numerical results. This is due to the inelastic and dissipative properties of "uncured" cement around 75–80 min curing time, which significantly delay the response time of the reflected solitary waves in experiments. Since the FEM model does not include inelastic and dissipative effects despite their obvious presence in experiments, particularly at early age, we observe smaller TOFs predicted by the numerical simulations compared to the experimental measurements. Once the cement becomes stiffer, there is an excellent agreement between the experimental and the numerical results. This demonstrates that our HNSW-based method is highly sensitive to the mechanical property of cement specimens as long as the local properties, i.e., close to the actuator, are identical to the bulk properties of the material.

The behavior of the amplitude ratio of the reflected solitary waves as a function of the Young's modulus presents similar trends. However, in this case the experimental results present smaller amplitudes than the numerical results because of the presence of dissipation (not accounted for in the numerical model). In the future, we expect that taking the dissipation into account and using more sophisticated numerical models [5] will enable a more detailed description of the HNSW attenuation during the hydration of cement-based materials.

6. Discussion and conclusions

This paper describes a nondestructive testing method based on the propagation of highly nonlinear solitary waves (HNSWs) as acoustic information carriers to monitor the hydration of quick-setting cement. A cost-effective actuator/sensor made of a chain of spherical particles (i.e., a granular crystal) and an electromagnet were used for the generation and detection of the HNSWs. A numerical and experimental study was conducted and compared to the results of a standard compression test. It was found that a single pulse perpendicularly incident to the actuator/cement interface results in a series of reflected pulses, categorized into a primary solitary wave (PSW) and a secondary solitary wave (SSW). The amplitudes and the time-of-flight (TOF) of these two reflected waves are strongly dependent on the stiffness of the cement. The experimental findings from the HNSW measurements were supported by a simplified finite element model that captured the sensitivity of the proposed HNSW-based method to the change of cement's elastic modulus. The experimental results obtained using HNSWs were also in agreement with experimental data obtained using conventional mechanical tests performed according to the ASTM C109.

The non-destructive approach proposed here provides advantages over conventional methods based on linear ultrasonic bulk waves. With respect to the ultrasonic pulse velocity (UPV) method, the present approach requires only one transducer (instead of at least two), and therefore, it allows simpler access to the test specimen. With respect to the wave reflection method, where the wave propagating within the buffer material experiences a change in the reflection coefficient due to cement age, the present approach can virtually exploit three parameters: (1) the time of flight (TOF) of the primary reflected waves, (2) the TOF of the secondary reflected waves, and (3) the amplitude of the reflected waves. Moreover the HNSW-based method does not require the use of electronics for the generation of high-voltage input signals, contrary to piezoelectric transducers. It is acknowledged that the method presented in this paper assumes that hydration is uniform in the whole cement sample, by providing "effective" materials properties near the surface. If hydration conditions are such that the mechanical properties of the material in the near field, i.e., close to the actuator, are significantly different than in the far field, the HNSWs-based features may not be representative of the whole structure. Further studies are planned to address the inhomogeneous, viscoelastic nature of cement in response to incident HNSWs. Future development may include the partial re-design of the tube containing the chain of particles in order to remove the thin sheet that currently prevents the bottom particle of the chain from falling into the fresh concrete. If the sheet is too thin it would deform permanently under the chain's weight. A thick sheet thick would be too rigid and therefore it would reduce the effect of the cement paste on the characteristics of the solitary waves.

Acknowledgements

This work was supported by the National Science Foundation grant CMMI—0825983 (Dr. Eduardo Misawa, Program Director). CD also acknowledges support from NSF/CMMI-0844540 (Career). PR and XN also thank the 2009 American Society for Nondestructive Testing Fellowship Award. We thank Dr. Julie Vandenbossche at the University of Pittsburgh for the usage of the Test Mark equipment.

References

[1] Van Den Abeele K, Desadeleer W, De Schutter G, Wevers M. Active and passive monitoring of the early hydration process in concrete using linear and nonlinear acoustics. Cem Concr Res 2009;39(5):426–32.
[2] Zhu J, Kee S.H. Monitoring early age microstructure development of cement paste using bender elements. Proc SPIE 2010; 7649: 76491R.
[3] Sayers CM, Grenfell RL. Ultrasonic propagation through hydrating cements. Ultrason 1993;31(3):147–53.
[4] Smith A, Chotard T, Gimet-Breart N, Fargeot D. Correlation between hydration mechanism and ultrasonic measurements in an aluminous cement: effect of setting time and temperature on the early hydration. J Eur Ceram Soc 2002;22(12):1947–58.
[5] Voigt T, Ye G, Sun Z, Shah SP, van Breugel K. Early age microstructure of Portland cement mortar investigated by ultrasonic shear waves and numerical simulation. Cem Concr Res 2005;35(5):858–66.
[6] Stepišnik J, Lukač M, Kocuvan I. Measurement of cement hydration by ultrasonics. Am Ceram Soc Bull 1981;64(4):481–3.
[7] Rao PP, Sutton DL, Childs JD, Cunningham WC. An ultrasonic device for nondestructive testing of oilwell cements at elevated temperatures and pressures. J Pet Technol 1982;34(11):2611–6.
[8] Keating J, Hannant DJ, Hibbert AP. Comparison of shear modulus and pulse velocity techniques to measure the build-up of structure in fresh cement pastes used in oil well cementing. Cem Concr Res 1989;19(4):554–66.
[9] Keating J, Hannant DJ, Hibbert AP. Correlation between cube strength, ultrasonic pulse velocity and volume change for oil well cement slurries. Cem Concr Res 1989;19(5):715–26.
[10] Sayers CM, Dahlin A. Propagation of ultrasound through hydrating cement pastes at early times. Adv Cem Based Mater 1993;1(1):12–21.
[11] D'Angelo R, Plona TJ, Schwartz LM, Coveney P. Ultrasonic measurements on hydrating cement slurries: onset of shear wave propagation. Adv Cem Based Mater 1995;2(1):8–14.
[12] Boumiz A, Vernet C, Tenoudji FC. Mechanical properties of cement pastes and mortars at early ages: evolution with time and degree of hydration. Adv Cem Based Mater 1996;3(3–4):94–106.
[13] Valič MI. Hydration of cementitious materials by pulse echo USWR: method, apparatus and application examples. Cem Concr Res 2000;30(10): 1633–40.
[14] Chotard T, Gimet-Breat N, Smith A, Fargeot D, Bonnet JP, Gault C. Application of ultrasonic testing to describe the hydration of calcium aluminate cement at the early age. Cem Concr Res 2001;30(3):405–12.
[15] Ye G, van Breugel K, Fraaij ALA. Experimental study and numerical simulation on the formation of microstructure in cementitious materials at early age. Cem Concr Res 2003;33(2):233–9.
[16] ′ztürk T, Kroggel O, Grübl P, Popovics JS. Improved ultrasonic wave reflection technique to monitor the setting of cement-based materials. NDT&E Int 2006;39(4):258–63.
[17] Punurai W, Jarzynski J, Qu J, Kurtis KE, Jacobs LJ. Characterization of entrained air voids in cement paste with scattered ultrasound. NDT&E Int 2006;39(6):514–24.
[18] Zhang J, Qin L, Li Z. Hydration monitoring of cement-based materials with resistivity and ultrasonic methods. Mater Struct 2009;42(1):15–24.
[19] Yu QL, Brouwers HJH., Korte de ACJ. Gypsum hydration: a theoretical and experimental study. In: 17th International Conference on Building Materials, ibausil, Weimar, Germany; 2009.
[20] Moukwa M, Brodwin M, Christo S, Chang J, Shah SP. The influence of the hydration process upon microwave properties of cements. Cem Concr Res 1991;21(5):863–72.
[21] El Hafiane Y, Smith A, Bonnet JP, Abelard P, Blanchart P. Electrical characterization of aluminous cement at the early age in the 10 Hz–1 GHz frequency range. Cem Concr Res 2000;30(7):1057–62.
[22] Naik TR, Malhotra VM, Popovics JS. The ultrasonic pulse velocity method. In: Malhotra VM, Carino NJ, editors. Handbook on Nondestructive Testing of Concrete. Boca Raton: CRC Press; 2004.
[23] Nesterenko VF. Propagation of nonlinear compression pulses in granular media. J Appl Mech Tech Phys 1984;24(5):733–43.
[24] Nesterenko VF. Dynamics of heterogeneous materials. New York: Springer-Verlag; 2001.
[25] Coste C. Falcon E, Fauve S. Solitary waves in a chain of beads under Hertz contact. Phys Rev E 1997;56(5):6104–17.
[26] Daraio C, Nesterenko VF, Herbold EB, Jin S. Strongly nonlinear waves in a chain of Teflon beads. Phys Rev E 2005;72(1):016603.
[27] Daraio C, Nesterenko VF. Strongly nonlinear wave dynamics in a chain of polymer coated beads. Phys Rev E 2006;73(2):026612.
[28] Daraio C, Nesterenko VF, Herbold EB, Jin S. Tunability of solitary wave properties in one-dimensional strongly nonlinear phononic crystals. Phys Rev E 2006;73(2):026610.
[29] Ni X, Rizzo P., Daraio C. Novel sensor technology for NDE of concrete. Proc. SPIE 2009; 7292: 729218.
[30] Spadoni A, Daraio C. Generation and control of sound bullets with a nonlinear acoustic lens. Proc Natl Acad Sci 2010;107(16):7230–4.
[31] Ni X, Rizzo P, Daraio C. Actuators for the generation of highly nonlinear solitary waves. Rev Sci Instrum 2011;82:034902.
[32] Manciu FS, Sen S. Secondary solitary wave formation in systems with generalized Hertz interactions. Phys Rev E 2002;66:016616.
[33] Falcon E, Laroche C, Fauve S, Coste C. Collision of a 1-D column of beads with a wall. Eur Phys J B 1998;5(1):111–31.
[34] Job S, Melo F, Sokolow A, Sen S. How Hertzian solitary waves interact with boundaries in a 1D granular medium. Phys Rev Lett 2005;94(17): 178002.
[35] Yang J, Silvestro C, Khatri D, De Nardo L, Daraio C. Interaction of highly nonlinear solitary waves with linear elastic media. Phys Rev E 2011;83: 046606.
[36] ASTM C 109/C 109M–08. Standard test method for compressive strength of hydraulic cement mortars.

[37] Ni X, Rizzo P, Daraio C. Laser-based excitation of nonlinear solitary waves in a chain of beads. Phys Rev E 2011;84(026601):5.
[38] Porter MA, Daraio C, Szelengowicz I, Herbold EB, Kevrekidis PG. Physica D 2009;238:666.
[39] Simulia. Abaqus version 6.8 Documentation. Providence: Dassault Systemes S.A.; 2008.
[40] Khatri D, Daraio C. Finite element modeling of highly nonlinear acoustic pulses using abaqus. In review.
[41] Carretero-González R, Khatri D, Porter MA, Kevrekidis PG, Daraio C. Dissipative solitary waves in granular crystals. Phys Rev Lett 2009;102(2): 024102.